Mathematical Modeling of Porosity Formation in Solidification

KIMIO KUBO and ROBERT D. PEHLKE

Shrinkage porosity and gas porosity occur simultaneously and at the same location when conditions are such that both may exist in a solidifying casting. Porosity formation in a solidifying alloy is described numerically, including the possible evolution of dissolved gases. The calculated amount and size of the porosity formed in Al-4.5 pct Cu plate castings compares favorably with measured values. The calculated distribution of porosity in sand cast Al-4.5 pct Cu plates of 1.5 cm thickness matches experimental measurements. The decrease of the hydrogen content by strong degassing and the increase of mold chilling power are recommended to produce sound aluminum alloy castings. The calculated results for steel plate castings are in agreement with the experimental work of Pellini. The present modeling has clarified the basis of empirical rules for soundness and suggests that the simultaneous occurrence of shrinkage and gas evolution is an essential mechanism in the formation of porosity defects.

I. INTRODUCTION

POROSITY defects such as shrinkage and gas holes are often found in castings. Although there are many reports[1-4] about computer simulation of macroscopic heat flow in castings, these modeling efforts do not predict porosity defects directly. There are some reports[5-8] which do predict the occurrence of shrinkage porosity from the pressure drop during interdendritic fluid flow. However, the effects of gases in solidifying metals have not been considered satisfactorily. In fact, formation of shrinkage porosity and gas holes in separate locations is rare, and when conditions for both to form exist, they occur simultaneously at the same place. In the present work, porosity formation in solidifying alloys is calculated numerically and includes consideration of shrinkage and gas evolution. The computer simulation should improve the capability of producing sound castings.

II. CONCEPT OF POROSITY FORMATION

Schematic representation of a possible feeding mechanism proposed by Campbell[6] is shown in Figure 1, where four types of feeding are illustrated. The first is liquid feeding which occurs at the initial stage of solidification. The second is mass feeding which may occur, but is not well understood. The third is interdendritic feeding which occurs at a later stage of solidification and may have direct effects on formation of porosity defects. The fourth is solid feeding which occurs at the last stage of solidification and is related to distortion of castings.

Porosity defects are caused by the limitations of these feeding mechanisms. Since the resistance to liquid feeding and mass feeding are small because they occur at low solid fraction, interdendritic feeding is considered to be the most important stage for creation of porosity defects. In this paper, porosity formation is analyzed only during the interdendritic feeding regime.

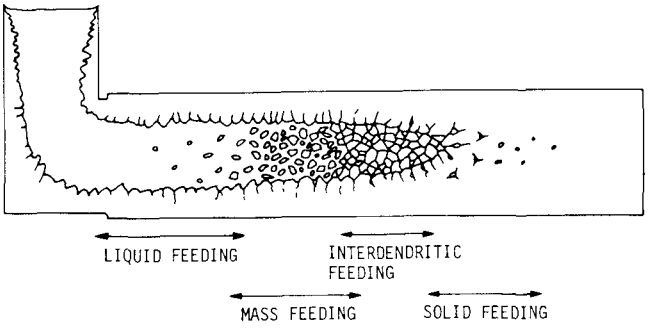

Fig. 1—Schematic representation of possible feeding mechanisms by Campbell [6]

Typical examples of porosity in castings of Al-4.5 pct Cu and Cu-8 pct Sn are shown in Figure 2. In Al-4.5 pct Cu round porosity defects are observed between secondary dendrite arms and at grain boundaries. In Cu-8 pct Sn dispersed small pores are found at the roots of the secondary arms, and continuous porosity is found at grain boundaries. These types of porosity are considered to form not only by lack of interdendritic feeding, but also by gas rejection into the liquid during solidification.

The growth process of porosity formation is illustrated schematically in Figure 3. At first, gas porosity nucleates at the roots of the secondary dendrite arms as shown in Figure 3(a). The free energy change on formation of porosity is

$$\Delta G = V(P_g - P) + A_1\sigma_{SG} + A_2\sigma_{LG} - A_1\sigma_{SL} \quad [1]$$

where V is the volume of porosity, P_g and P are gas pressure and metal pressure, A_1 and A_2 are the areas of solid-gas and liquid-gas interface, and σ_{SG}, σ_{LG}, and σ_{SL} are solid-gas, liquid-gas, and solid-liquid interfacial energies, respectively. When gas porosity forms at equilibrium, ΔG is zero. The first term on the right side of Eq. [1] represents the free energy change in going from liquid to gas porosity. The other terms represent the excess free energy change necessary to form the gas porosity surface. In homogeneous nucleation, the first term is required to be a very large negative value to overcome the effect of the gas porosity surface energy as reported by Fisher.[9] However, in this case, since the effect of surface energy is reduced by $A_1\sigma_{SL}$, a large

KIMIO KUBO is Visiting Assistant Research Scientist on leave from Osaka University, Osaka, Japan. ROBERT D. PEHLKE is Professor, Department of Materials and Metallurgical Engineering, University of Michigan, Ann Arbor, MI 48109

Manuscript submitted August 29, 1984.

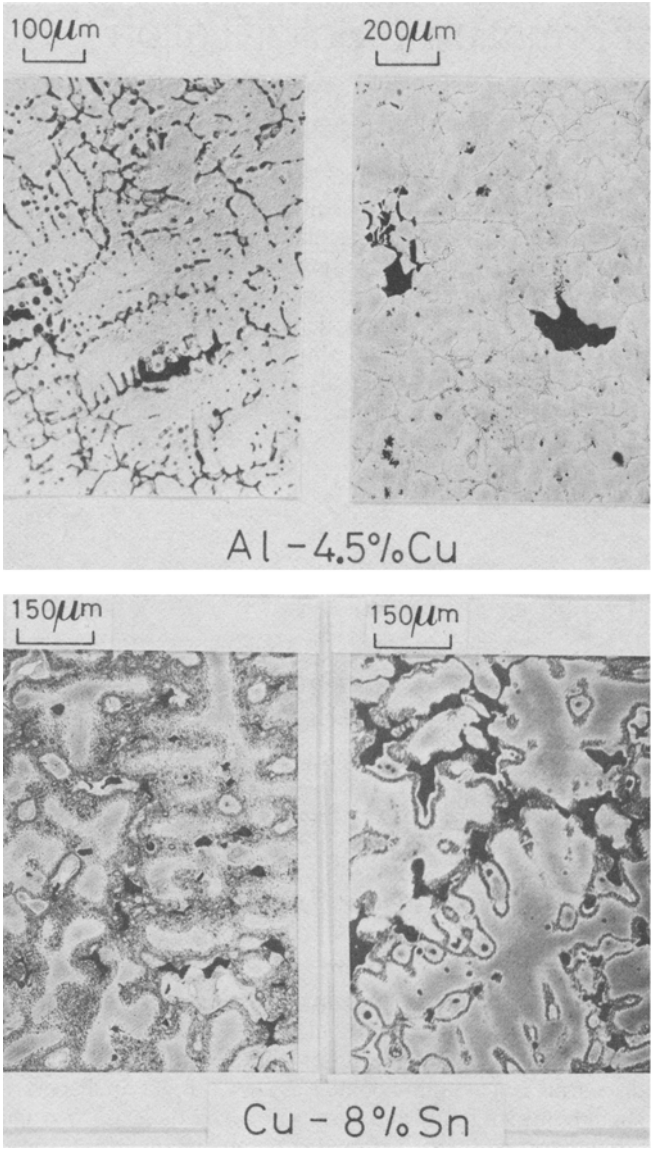

Fig. 2—Porosity in solidified alloys

negative pressure is not required. Consequently, porosity nucleates easily at the location shown in Figure 3(a).

With the progress of solidification, the gas dissolved in the liquid increases and the porosity grows. Since the radius of the porosity becomes large enough to decrease the contribution of interfacial energies, the porosity can detach from the dendrite as shown in Figure 3(b). Buoyant and convective forces promote this detachment. Furthermore, at a later stage of solidification, the neighboring dendrites collide, so that interdendritic feeding becomes difficult. At that point, the porosity is assumed to grow to compensate for solidification shrinkage.

III. MATHEMATICAL MODELING

A. *Heat Balance Equation*

In another paper by the present authors,[10] a new model was proposed to express microscopical and macroscopical temperature and composition in dendritic solidification. It

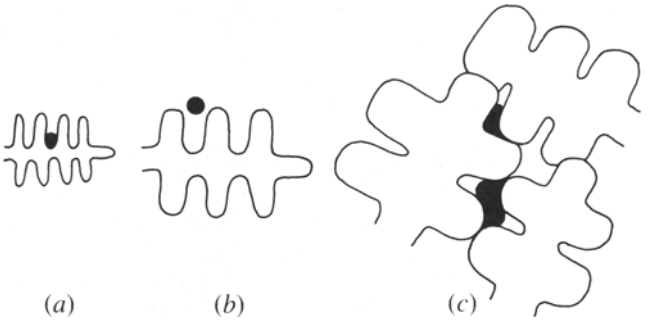

Fig. 3—Growth process of porosity formation

indicated that although the heat flow in dendritic solidification is microscopically three dimensional, the temperature in a volume element can be assumed to be uniform in considering macroscopic heat flow.

For purposes of this development, a two dimensional field is considered, and constant thermal properties are assumed. The heat balance equation is expressed as

$$C\rho\frac{\partial T}{\partial t} + f_L C\rho\left(u\frac{\partial T}{\partial x} + v\frac{\partial T}{\partial y}\right) = \lambda\left(\frac{\partial^2 T}{\partial x^2} + \frac{\partial^2 T}{\partial y^2}\right) - \rho L\frac{\partial f_L}{\partial t} \quad [2]$$

where ρ is an average density of liquid and solid being expressed as $f_L\rho_L + f_S\rho_S$. ρ_L and ρ_S are used as ρ for the fully liquid and solid regions, respectively. Since the specific heat and the thermal conductivity of solid and liquid at the melting point for most casting alloys are not known well, they are assumed to be independent of temperature and equal for the two phases. The first term on the left side of Eq. [2] is the heat accumulation, and the second term is the heat flux by interdendritic flow. The first term on the right side of Eq. [2] is the heat flux by conduction, and the second term is the evolved latent heat. The temperature gradients are small in the mushy zone and the liquid fraction is relatively small, and therefore, the temperature terms for interdendritic flow can be neglected. Also, the effects of slight changes in solute concentration on the energy balance are negligible. Equation [2] reduces to

$$\frac{\partial T}{\partial t} = \frac{\lambda}{C\rho}\left(\frac{\partial^2 T}{\partial x^2} + \frac{\partial^2 T}{\partial y^2}\right) - \frac{L}{C}\frac{\partial f_L}{\partial t} \quad [3]$$

To solve Eq. [3] the relationship between liquid fraction and temperature is needed. One limit of the relationship is obtained by assuming complete equilibrium. From the lever rule it is expressed as

$$f_L = \frac{C_0 m_L - k_0(T - T_m)}{T - T_m - k_0(T - T_m)} \quad [4]$$

The other limit is obtained from Scheil's equation which ignores solid diffusion as[11]

$$f_L = \left(\frac{T - T_m}{m_L C_0}\right)^{1/(k_0 - 1)} \quad [5]$$

Another paper[10] indicates that the relationship for Al-4.5 pct Cu alloy is close to Scheil's equation even for low cooling rates. In this development, Eq. [4] is used for steel and Eq. [5] is used for Al-4.5 pct Cu alloy, since the diffusivity of carbon in solid iron ($5.9 \cdot 10^{-9}$ m^2 per second at

1809 K)[12] is higher by three orders of magnitude than that of Cu in solid aluminum ($1.5 \cdot 10^{-12}$ m^2 per second at 933 K).[13]

B. *Continuity Equation*

From a mass balance for a volume element, the continuity equation requires

$$\left(\frac{\rho_S}{\rho_L} - 1\right)\frac{\partial f_L}{\partial t} - \frac{\partial f_L u}{\partial x} - \frac{\partial f_L v}{\partial y} + \frac{\partial f_s}{\partial t} = 0 \qquad [6]$$

The first term on the left side of Eq. [6] is the amount of shrinkage, and the second and third terms are the amount of liquid input by interdendritic flow. The last term is the amount of porosity growth. Equation [6] indicates that the shrinkage during solidification is compensated by interdendritic flow and the growth of porosity.

C. *Motion Equation*

The motion equation describing interdendritic flow can be expressed from Darcy's law as[11]

$$u = -\frac{k}{\mu f_L}\frac{\partial P}{\partial x} \qquad [7]$$

$$v = -\frac{k}{\mu f_L}\frac{\partial P}{\partial y} - \frac{k\rho g}{\mu f_L} \qquad [8]$$

where k is permeability, being calculated from the liquid fraction, f_L and dendrite cell size, d as[10,14]

$$k = \frac{f_L^3 d^2}{180(1 - f_L)^2} \qquad [9]$$

When f_L is larger than 0.7, the value obtained by substituting 0.7 into Eq. [9] has been used in calculations. When f_L is less than 0.01, that obtained by substituting 0.01 has been used. The region where feeding is controlled by interdendritic flow has not been distinguished from other regions. The following relationship[11] between the dendrite cell size and the local solidification time has been used to calculate the permeability by Eq. [9].

$$d = a\,\Delta\theta_f^n \qquad [10]$$

Before solidification is initiated, a time increment for the numerical calculation is substituted in Eq. [10].

Gas pressure in the porosity should balance with the metal pressure and the liquid-gas surface energy as[11]

$$P_g = P + \frac{2\sigma_{LG}}{r} \qquad [11]$$

In this development, the diameter of porosity forming first is assumed to be the same as the dendrite cell size. When the solidification rate is extremely large, Eq. [11] is not satisfied because of very small values of r. Generally in dendritic solidification, the cell size is more than ten micrometers, so it is rare that gaseous solute is trapped completely in the solid, except at very low gas contents.

D. *Conservation Equation of Gas Content*

1. *Hydrogen in an aluminum alloy*

Hydrogen alone can dissolve in an aluminum alloy. The diffusivity of hydrogen in solid aluminum at 933 K is ($2.0 \cdot 10^{-7}$ m^2 per second)[29] which is much larger than that of copper ($1.5 \cdot 10^{-12}$ m^2 per second).[13] In this case, assuming complete equilibrium, the conservation equation for gas content is expressed as

$$[H_0] = (1 - f_L)[H_s] + f_L[H_L] + \alpha_H\frac{P_g f_s}{T} \qquad [12]$$

The left side of Eq. [12] is the initial hydrogen content. The first, second, and third terms on the right are the amounts of hydrogen in the solid, liquid, and porosity, respectively. The hydrogen content in the solid and liquid are expressed as

$$[H_s] = K_{SH}P_g^{1/2} \qquad [13]$$

$$[H_L] = K_{LH}P_g^{1/2} \qquad [14]$$

2. *CO in steel*

CO gas is the main origin of gas porosity in steel. Although nitrogen may also be a source, it normally exhibits minor effects. In the present case, CO gas is assumed to be the only source of gas porosity. However, CO is a chemical compound, and the treatment of CO solubility is somewhat complex.

At first, CO gas is formed by the reaction of dissolved carbon and oxygen in steel as

$$[C_L] + [O_L] = CO \qquad [15]$$

Then, the gas pressure of CO is expressed as

$$P_g = [C_L][O_L]/K_{CO} \qquad [16]$$

The diffusivities of carbon and oxygen in solid steel at solidification temperatures are $5.9 \cdot 10^{-9}$ and $6.0 \cdot 10^{-9}$ m^2 per second, respectively.[12] These values are much larger than that of copper in aluminum ($1.5 \cdot 10^{-12}$ m^2 per second).[13] Assuming complete equilibrium, a mass balance for carbon and oxygen can be expressed as

$$[C_0] = [C_L]f_L + [C_S]f_S + \alpha_C\frac{P_g f_s}{T} \qquad [17]$$

$$[O_0] = [O_L]f_L + [O_S]f_S + \alpha_0\frac{P_g f_s}{T} + \beta\Delta SiO_2 \qquad [18]$$

The carbon and oxygen contents of the solid are expressed as

$$[C_S] = k_{Fe\text{-}C}[C_L] \qquad [19]$$

$$[O_S] = k_{Fe\text{-}O}[O_L] \qquad [20]$$

As Turkdogan[15] reported, with the progress of solidification the oxygen content in the liquid increases, so deoxidation reactions occur, as for example in the case of formation of silica.

$$[Si] + 2[O_L] = SiO_2 \qquad [21]$$

In this work the effect of manganese has been ignored to simplify this illustrative example. In Eq. [21], the equilibrium partition ratio is assumed to be unity. The oxygen and silicon contents in the liquid can be expressed as

$$[O_L]^2 = K_{SiO_2}/[Si] \qquad [22]$$

$$[Si] = [Si_0] - \beta\Delta SiO_2 \qquad [23]$$

As described later, Eqs. [16] through [18], [22], and [23] are solved simultaneously to obtain P_g or f_s.

E. *Flow Chart for Algorithm of Calculation*

A flow chart for the calculation algorithm is shown in Figure 4. At first the temperature of a volume element and the change of solid fraction are calculated from Eq. [3] by an implicit finite difference method. If the volume element is in the mushy zone, the variables are calculated in the following manner.

When no porosity has formed, the metal pressure, P, is calculated from Eqs. [6] through [8] by the implicit finite difference method, assuming no occurrence of porosity. Upwind Differencing[16] is applied to the interdendritic flow. The gas pressure, P_g, is calculated from Eq. [11], assuming the diameter of porosity forming first being the dendrite cell size. Subsequently, a new amount of porosity is calculated from Eqs. [12] through [14] for hydrogen gas porosity and from Eqs. [16] through [20], [22], and [23] for CO gas porosity.

When porosity has already formed, the flux of liquid by interdendritic fluid flow is calculated by the explicit finite difference method from Eqs. [6] through [8]. When the flux of liquid is positive, P and P_g are calculated from Eqs. [6] through [8] and [11], respectively, using f_v^B which is the amount of porosity before the current Δt (time increment).

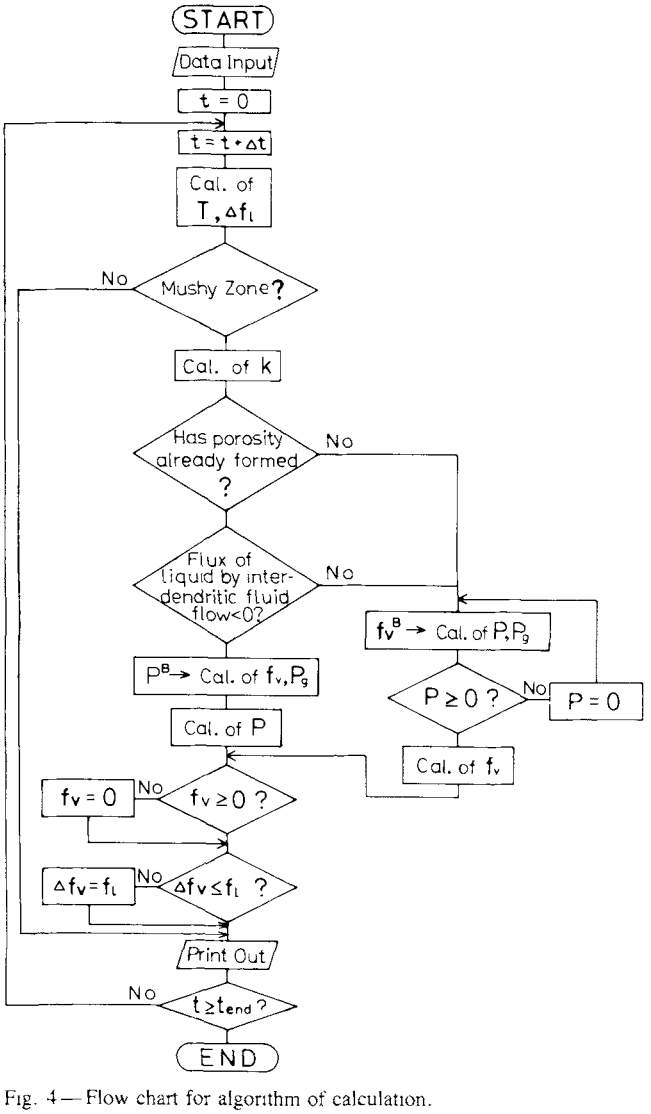

Fig. 4—Flow chart for algorithm of calculation.

Subsequently, a new value for f_v is calculated from Eqs. [12] through [14] for hydrogen gas porosity and from Eqs. [16] through [20], [22], and [23] for CO gas porosity.

When the flux of liquid by interdendritic flow is negative, f_v is calculated from Eqs. [6] through [8] by the explicit finite difference method using P^B which is the metal pressure before the current Δt. P_g is calculated from Eqs. [12] through [14] for hydrogen gas porosity and from Eqs. [16] through [20], [22], and [23] for CO gas porosity. Then, a new value of P is calculated from Eq. [11].

When f_v and P become negative, they are corrected to zero. When the increase of porosity becomes larger than the liquid fraction, it is corrected to be equal to the liquid fraction.

The procedure described above is repeated over each volume element and each time step until the required time is reached.

F. *Constants and Properties Used in Calculation*

The castings analyzed are plates with an end feeder, and it is assumed that heat transfer to the mold can be described as a metal-mold interface which is uniformly cooled by convection except at the top of the feeder. The heat transfer coefficient, h, is assumed to be 420 and 42 $W/m^2 \cdot K$ which correspond approximately to the cooling rates of a metallic mold and a sand mold, respectively. Calculations were carried out with various time increments, Δt, until the results were identical for Δt less than a certain value depending on the coefficient of heat transfer. In this paper the results with a sufficiently small Δt are shown. The constants and properties[15,17-23] used for Al-4.5 pct Cu and steel (0.14 pct C, 0.3 pct Si) are shown in Table I.

IV. RESULTS AND DISCUSSION

A. *Al-4.5 Pct Cu Plate Castings*

The calculated amount of porosity in Al-4.5 pct Cu plate castings is shown in Figure 5. Figure 5(a) shows the case of an initial hydrogen content of 0.3 cc/100 g and a heat transfer coefficient of 42 $W/m^2 \cdot K$ (sand mold). The amount of porosity is more than 3 pct over the entire plate. In the case of a hydrogen content of 0.2 cc/100 g, the amount of porosity decreases considerably as shown in Figure 5(b). On the other hand, in the case of a heat transfer coefficient of 420 $W/m^2 \cdot K$ (metallic mold), the amount of porosity also decreases considerably even at the higher hydrogen content of 0.3 cc/100 g as shown in Figure 5(c). The amount of porosity of a thinner plate also decreases even at the higher hydrogen content and at a lower cooling rate as shown in Figure 5(d). In this case, the amount of porosity near the end away from the feeder becomes very small. Deoras and Kondic[24] (pure aluminum and aluminum silicon alloys) and Nishi and Kurobuchi[23] (Al-4.5 pct Cu) reported that the amounts of porosity increase rapidly when the hydrogen content is more than 0.2 cc/100 g. Nishi, *et al.*[25] also reported that the amounts of porosity for a sand mold are 1.0 pct and 0.5 pct at 0.3 cc/100 g and 0.2 cc/100 g of hydrogen content, respectively. On the other hand, those for a metallic mold are 0.3 pct and 0.1 pct at 0.3 cc/100 g and 0.2 cc/100 g, respectively. The calculated results of this investigation are in good qualitative agreement with these experimental results.

Table I. Constants and Properties

	Al-4.5 Pct Cu	Steel
Specific heat, C (kJ/kg · K)	1.09	0.72
Thermal conductivity, λ (W/m · K)	210	33
Density of liquid, ρ_L (kg/m^3)	2380	7210
Density of solid, ρ_S (kg/m^3)	2520	7430
Latent heat of fusion, L (kJ/kg)	394	272
Liquidus slope, m_L (K/wt pct)	−3.39	−80.39
Equilibrium partition ratio of copper in aluminum alloy, k_0	0.173	—
Equilibrium partition ratio of carbon in steel, $k_{Fe\text{-}C}$	—	0 20
Equilibrium partition ratio of oxygen in steel, $k_{Fe\text{-}O}$	—	0.076
Gas-Liquid interface energy, σ_{LG} (N/m)	0.914	1 70
Viscosity of liquid metal, (Pa · s)	4.5×10^{-3}	7.0×10^{-3}
Constant in Eq. [10], a	7.5×10^{-6}	1.49×10^{-5}
Constant in Eq. [10], n	0.39	0.39
Equilibrium constant, K_{SH} (cc/100 g · atm$^{1/2}$)	0 06	—
Equilibrium constant, K_{LH} (cc/100 g · atm$^{1/2}$)	0.6	—
Equilibrium constant, K_{CO} [(wt pct)^2/atm]	—	0 0023
Equilibrium constant, K_{SiO_2} [(wt pct)^3]	—	2.74×10^{-6}
Pouring temperature, T_p(K)	933	1807
Melting point of pure metal, T_m (K)	933	1807
Room temperature, T_0 (K)	293	293
Initial hydrogen content, [H_0] (cc/100 g)	0.2, 0.3	—
Initial carbon content in steel, [C_0] (wt pct)	—	0.14
Initial oxygen content in steel, [O_0] (wt pct)	—	0 003
Initial silicon content of steel, [Si_0] (wt pct)	—	0.3

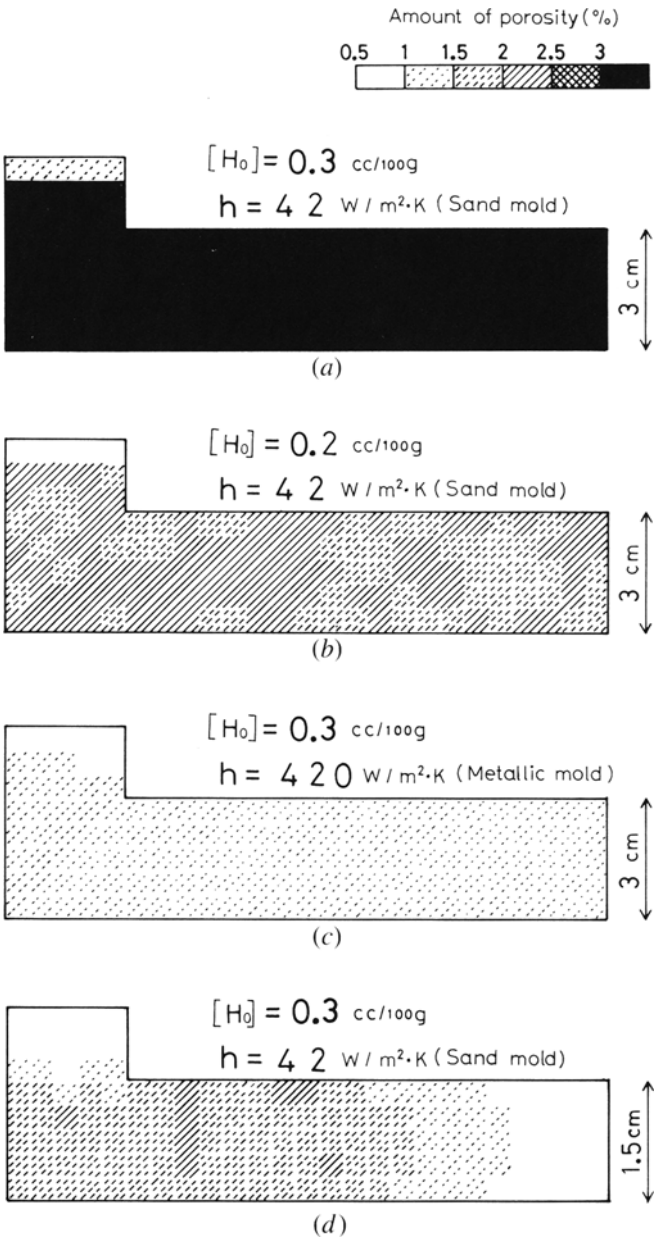

Fig 5 — Calculated amount of porosity in Al-4.5 pct Cu plate castings.

The calculated radius of the porosity in Al-4.5 pct Cu plate castings is shown in Figure 6. The range of the radius is from 10 μm to 40 μm. The radius of the porosity of a 3 cm thick plate, cooled by an h of 42 W/m^2 · K (sand mold), is large regardless of the initial hydrogen content (Figures 6(a) and (b)). It decreases for an h of 420 W/m^2 · K (metallic mold) and for a 1.5 cm thick plate (Figures 6(c) and (d)). These calculated results are in good qualitative agreement with experimental results for the radius of porosity (less than 20 μm for metallic molds, and as large as 100 μm for sand molds).[26]

The calculated change of amount and radius of porosity, metal pressure, and gas pressure with the solid fraction at the center of the plate are shown in Figure 7. The drop in metal pressure for a metallic mold is larger than that for a sand mold because the flux of liquid by interdendritic flow is larger for higher rates of solidification. The increase of metal pressure for the metallic mold at a solid fraction of about 0.75 is due to relief of the depression in pressure by formation of porosity.

The metal pressure for the sand mold is approximately atmospheric pressure up to a solid fraction of 0.8. As the resistance to interdendritic flow becomes larger after the solid fraction of 0.8, the metal pressure suddenly decreases. Consequently, the gas pressure in the porosity decreases and the amount of porosity increases accordingly. On the other hand, the gas pressure for the metallic mold does not decrease significantly, and the amount of porosity does not increase appreciably, *i.e.*, in a metallic mold, hydrogen gas at higher pressure exists in smaller size porosity than in a sand mold.

Distributions of the amount of porosity in Al-4.5 pct Cu plate castings of 1.5 cm thickness poured into a sand mold are shown in Figure 8. As the hydrogen content in the experiment was not measured, the calculated amounts can not be compared quantitatively with experiment. However, as indicated in Figure 8, both show a similar trend.

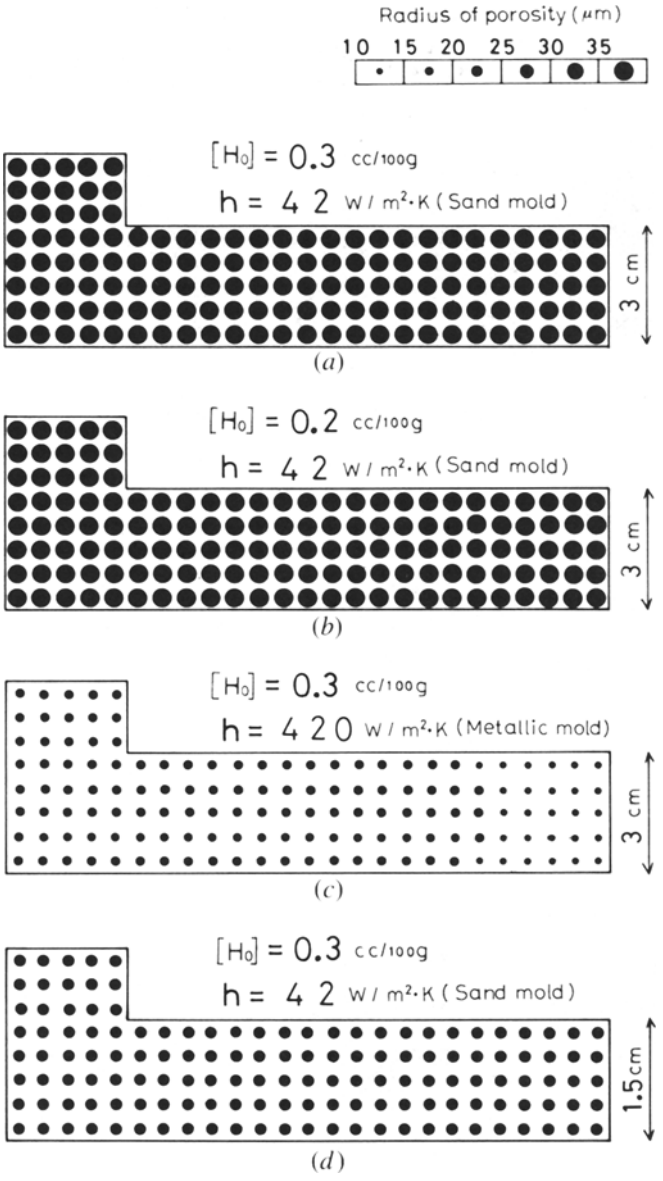

Fig 6—Calculated radius of porosity in Al-4 5 pct Cu plate castings

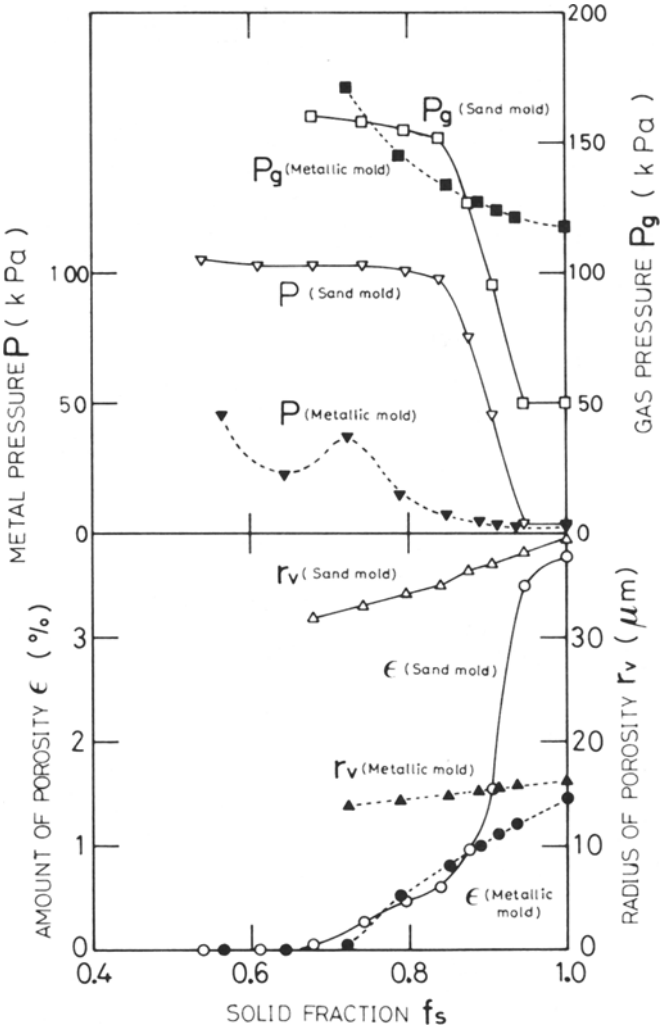

Fig 7—Calculated change of amount and radius of porosity, metal pressure, and gas pressure with solid fraction in Al-4 5 pct Cu plate castings at hydrogen content of 0 3 cc/100 g

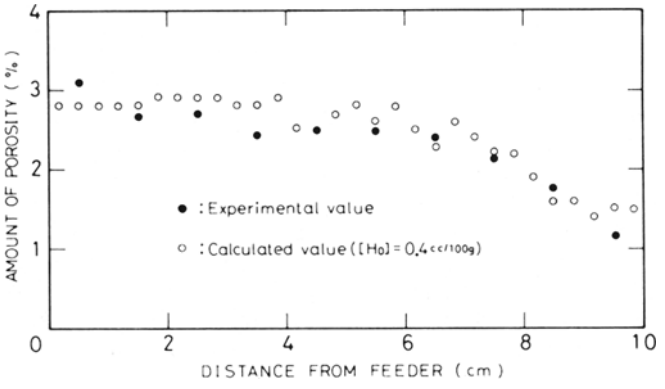

Fig 8—Distribution of amount of porosity in Al-4 5 pct Cu plate castings of 1 5 cm thickness poured into a sand mold

B. *Steel Plate Castings*

The calculated amount of porosity in steel plate castings (0.14 pct C, 0.3 pct Si) poured into sand molds is shown in Figure 9. The thickness of the plate, D, is 3 cm, and the ratios of D to the length from the end to the feeder, L, are 3, 4, and 6. When L/D is 3 or 4, severe porosity defects are not predicted. However, when L/D is 6, porosity up to 3 pct is predicted near the centerline. The calculation indicates that porosity defects do not occur within $2.5D$ from the end of the plate regardless of the value of L/D. Once porosity defects form, they spread near the feeder as shown in Figure 9(c). Pellini[27] reported that the maximum feeding distance for plates is $4.5D$ which is composed of an edge contribution of $2.5D$ and a feeder contribution of $2D$. Pellini's empirical rules have been used widely for casting designs.[28] The present modeling results coincide well with the experimental results obtained by Pellini.

The temperature and metal pressure distributions calculated at a later stage in solidification of steel plate castings poured into sand molds are shown in Figure 10. Indicated isotherms from 1761 K to 1755 K correspond to liquid fractions ranging from 5.6 pct to 2.0 pct where porosity defects form severely. When the porosity defects are absent (L/D = 3), the temperature gradient toward the feeder is more than about 2 K/cm. On the other hand, when the

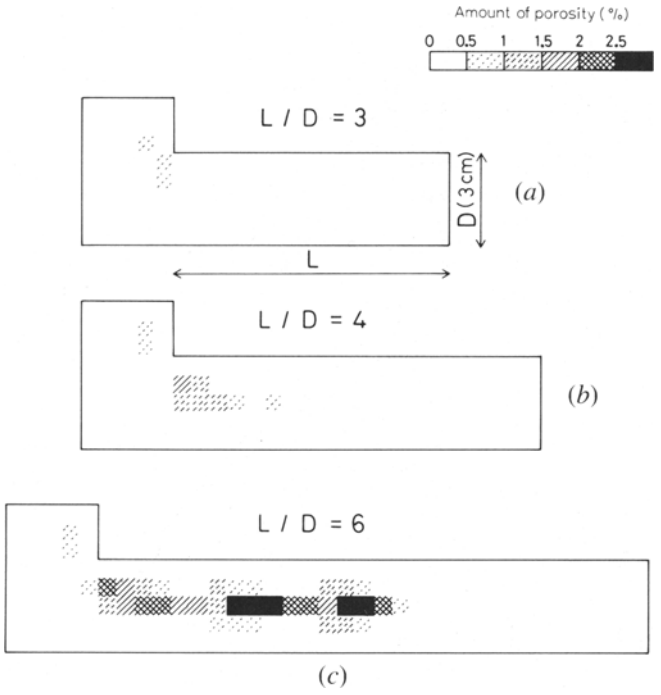

Fig. 9 — Calculated amount of porosity in steel plate castings (0.14 pct C, 0.30 pct Si) poured into sand molds

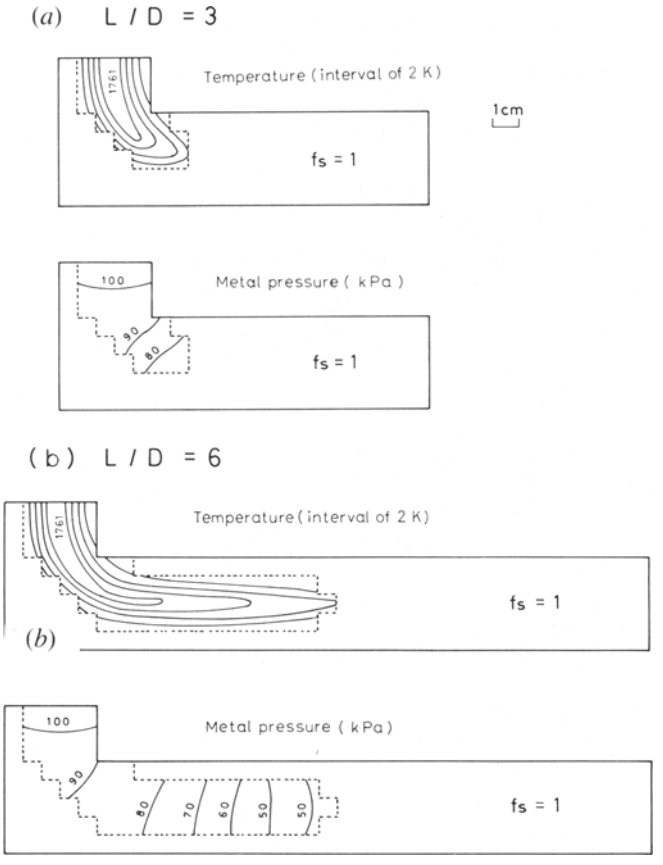

Fig. 10 — Calculated temperature and metal pressure distribution at a later stage of solidification of steel plate castings poured into sand molds

Fig. 11 — Interdendritic flow velocities calculated at a later stage in solidification of a steel plate casting poured into a sand mold

porosity defects occur, *e.g.*, at ($L/D = 6$), the temperature gradient toward the feeder is less than 1 K/cm. This result supports the opinion of Niyama, *et al.*[3] that the critical temperature gradient for occurrence of a shrinkage cavity in steel castings is 2 K/cm, which corresponds to a liquid fraction gradient of 0.012/cm. The metal pressure of the casting free from defects is 80 kPa at the point most distant from the feeder, whereas that of the casting containing defects is 50 kPa at this location. Since the metal pressure is low, CO gas porosity can easily form, particularly in combination with shrinkage.

The interdendritic flow velocities at a later stage of solidification of the steel plate casting poured into a sand mold are shown in Figure 11. This is for a case of occurrence of severe porosity defects. The direction of the vector of velocity is reversed near the point farthest from the feeder, *i.e.*, shrinkage during solidification is compensated by porosity growth at the point farthest from the feeder.

V. CONCLUSIONS

1. Formation of porosity in solidifying alloys has been modeled numerically, taking gas evolution and interdendritic flow into consideration.
2. The calculated distribution, amount, and radius of porosity in Al-4.5 pct Cu plate castings was in good qualitative agreement with experiment.
3. The proposed modeling has made the basis clear for empirical rules for soundness of steel castings, and suggests that the simultaneous occurrence of shrinkage and gas evolution is a key mechanism of porosity defect formation.
4. The minimization of gas content by degassing and increasing mold chilling power are recommended to produce sound castings. The recommended limiting gas content and mold chilling power depend on casting shape, alloy composition, required mechanical properties, and other foundry variables which require more detailed investigation for further quantification.

NOMENCLATURE

A_1	area of solid-gas interface (m^2)
A_2	area of liquid-gas interface (m^2)
a	constant in Eq. [10]
C	specific heat (kJ/kg · K)
$[C_0]$	initial carbon content in steel (wt pct)
$[C_l]$	carbon content in liquid (wt pct)

$[C_S]$ carbon content in solid (wt pct)
D thickness of plate casting (m)
d dendrite cell size (m)
f_L liquid fraction
f_S solid fraction
f_v porosity
Δf_S increase of solid fraction
Δf_v increase of porosity
ΔG free energy change on formation of porosity (J)
g acceleration of gravity (9.80 m/s^2)
$[H_0]$ initial hydrogen content in aluminum alloy (cc/100 g)
$[H_L]$ hydrogen content in liquid (cc/100 g)
$[H_S]$ hydrogen content in solid (cc/100 g)
h heat transfer coefficient (W/m^2 · K)
K_{CO} equilibrium constant of Eq. [13] ((wt pct)^2/atm)
K_{LH} equilibrium constant of Eq. [11] (cc/100 g · atm$^{1/2}$)
K_{SH} equilibrium constant of Eq. [10] (cc/100 g · atm$^{1/2}$)
K_{SiO_2} equilibrium constant of Eq. [19] ((wt pct)^3)
k permeability (m^2)
k_0 equilibrium partition ratio of copper in aluminum alloy
k_{Fe-C} equilibrium partition ratio of carbon in steel
k_{Fe-O} equilibrium partition ratio of oxygen in steel
L latent heat of fusion (kJ/kg)
m_L liquidus slope (K/wt pct)
n constant in Eq. [10]
$[O_0]$ initial oxygen content in steel (wt pct)
$[O_L]$ oxygen content in liquid (wt pct)
$[O_S]$ oxygen content in solid (wt pct)
P metal pressure (Pa)
P_g gas pressure (Pa)
r radius of porosity (m)
[Si] silicon content of steel (wt pct)
$[Si_0]$ initial silicon content of steel (wt pct)
ΔSiO_2 content of deoxidation product by silicon (wt pct)
T temperature (K)
T_0 room temperature (K)
T_m melting point of pure metal (K)
T_p pouring temperature (K)
t time (s)
Δt time increment (s)
u velocity in x direction (m/s)
V volume of porosity (m^3)
v velocity in y direction (m/s)
x coordinate (m)
y coordinate (m)
α_C constant in Eq. [14] $\left(\frac{0.146}{f_L\rho_L + f_S\rho_S}\right)$
α_H constant in Eq. [9] $\left(\frac{27300}{f_L\rho_L + f_S\rho_S}\right)$
α_O constant in Eq. [15] $\left(\frac{0.390}{f_L\rho_L + f_S\rho_S}\right)$
β constant in Eq. [15] (0.467)
$\Delta\theta_f$ local solidification time (s)
λ thermal conductivity (W/m · K)
μ viscosity of liquid metal (Pa · s)
ρ average density, $f_L\rho_L + f_S\rho_S$ (kg/m^3)
ρ_L density of liquid (kg/m^3)
ρ_S density of solid (kg/m^3)
σ_{LG} gas-liquid interfacial energy (N/m)
σ_{SG} gas-solid interfacial energy (N/m)
σ_{SL} solid-liquid interfacial energy (N/m)

superscript

B value before Δt

REFERENCES

1. A. Jeyarajan and R D Pehlke *Trans Amer Foundrymen's Soc.*, 1978, vol 86, pp. 457-64
2. W C Erickson *AFS Int Cast Metals J*, 1980, vol 5, no 1, pp 30-41
3. E Niyama, T Uchida, M Morikawa, and S Saito. *AFS Int Cast Metals J*, 1981, vol 6, no. 2, pp 16-22
4. I. Imafuku *Trans. Japan Soc of Mech Engrs, Ser C*, 1981, vol 47, pp 918-26
5. T S Piwonka and M C Flemings *Trans TMS-AIME*, 1966, vol 236, pp 1157-65
6. J Campbell, *AFS Cast Metals Res J*, 1969, vol 5, no 1, pp 1-8
7. V de L Davies *AFS Cast Metals Res J*, 1975, vol 11, no 2, pp 33-44
8. I Ohnaka, Y Mori, Y Nagasaka, and T Fukusako, *J Japan Foundrymen's Soc*, 1981, vol 53, pp 673-79
9. J C Fisher *J App Phys*, 1948, vol 19, pp 1062-67
10. K Kubo, R. D. Pehlke, and T Fukusako* The University of Michigan, Ann Arbor, MI and *Osaka University, Suita, Osaka, Japan, unpublished research, 1984.
11. M C Flemings, *Solidification Processing*, McGraw-Hill Book Co., New York, NY, 1974, pp 34, 148, 207, and 234
12. H Bester and K W Lange *Arch Eisenhüttenwes*, 1972, vol 43, pp 207-13
13. J B Murphy, *Acta Metall*, 1961, vol 9, pp 563-69
14. P C Carman: *Trans Inst Chem Eng*, 1937, vol 15, pp. 150-66
15. E T Turkdogan: *Trans TMS-AIME*, 1965, vol 233, pp 2100-12
16. P J. Roache *Computational Fluid Dynamics*, Hermosa Publishers, 1972, p 64
17. M Hansen *Constitution of Binary Alloys*, 2nd ed, McGraw-Hill Book Co, New York, NY, 1958, pp 84-90, 353-65
18. S Matoba, K Gunji, and T Kuwana *Tetsu to Hagané*, 1959, vol 45, pp 229-232
19. T F Bower, H D Brody, and M C Flemings, *Trans TMS-AIME*, 1966, vol 236, pp 624-34
20. T Z Kattamis, J C Coughlin, and M C. Flemings *Trans TMS-AIME*, 1967, vol 239, pp 1504-11
21. A. Suzuki, T Suzuki, Y Nagaoka, and Y Iwata *Tetsu to Hagané*, 1968, vol 32, pp 1301-05
22. K Mori, A Kamimori, M Deguchi, and T Shimoda, *Tetsu to Hagané*, 1973, vol 59, pp. 887-97
23. S Nishi and T Kurobuchi, *Keikinzoku*, 1974, vol 24, pp 245-54
24. B.R Deoras and V. Kondic *Foundry Trade J*, 1956, vol. 100, pp 361-64
25. S Nishi, Y Shinada, and T. Kurobuchi, *Keikinzoku*, 1974, vol 24, pp 130-34
26. K Kubo, T Fukusako, and I Ohnaka *J Japan Foundrymen's Soc*, 1979, vol. 51, pp 586-91
27. W. S Pellini, *Trans Amer Foundrymen's Soc*, 1953, vol 61, pp 61-80
28. P R Beely *Foundry Technology*, Butterworths, London, 1972, p 112
29. C E Ransley and D E Talbot, *Z Metallknde*, 1955, vol 46, p 328